Structure of the Pb, Bi, Th, and U *M* x-ray spectra

Silvina P. Limandri and Jorge C. Trincavelli
Facultad de Matemática, Astronomía y Física, Universidad Nacional de Córdoba, Ciudad Universitaria, 5000, Córdoba, Argentina and Consejo Nacional de Investigaciones Científicas y Técnicas of the Argentine Republic, Buenos Aires, Argentina

Rita D. Bonetto
Centro de Investigación y Desarrollo en Ciencias Aplicadas Dr. Jorge Ronco, Calle 47 No 257, CC 59, 1900 La Plata, Argentina; Facultad de Ciencias Exactas y Facultad de Ingeniería, Universidad Nacional de La Plata, La Plata, Argentina; and Consejo Nacional de Investigaciones Científicas y Técnicas of the Argentine Republic, Buenos Aires, Argentina

Alejo C. Carreras
Instituto de Investigaciones en Tecnología Química (INTEQUI), Universidad Nacional de San Luis CC290-5700, San Luis, Argentina and Consejo Nacional de Investigaciones Científicas y Técnicas of the Argentine Republic, Buenos Aires, Argentina

(Received 22 July 2008; published 29 August 2008)

The emission of x rays in atomic transitions from *M*-shell vacancy states of Pb, Bi, Th, and U induced by electron bombardment was studied by means of wavelength dispersive spectroscopy. Relative transition probabilities, characteristic energies, natural linewidths, and x-ray production cross sections were determined through a careful spectral processing based on a parameter refinement method. The experimental data for a number of *M*-shell relative transition probabilities along with values for a large set of atomic parameters are given. Finally, the origin and shape of the satellite bands at the high-energy side of the main lines are discussed.

DOI: 10.1103/PhysRevA.78.022518 PACS number(s): 32.30.Rj, 32.70.−n, 33.70.Jg, 34.80.Dp

I. INTRODUCTION

Characteristic x-ray emission spectra contain valuable information about some features of atomic and molecular structures. Comparisons between calculated and measured x-ray spectra are often performed in order to test theoretical predictions based on some approximations assumed in different atomic models.

The processing and analytical description of experimental spectra allows one to determine a number of absolute parameters, which represent quantities of interest in the field of atomic physics. In addition, a detailed knowledge of the characteristics of these emission spectra is very useful due to its applicability in several spectroscopic techniques based on the analysis of x rays emitted by a specimen as a consequence of the interaction processes of radiation with matter.

Information is scarce in the literature concerning the structure of the *M*-line spectra of heavy elements because the features of *M*-line emission are not well known due to some theoretical and experimental difficulties related to the complexity of the more external atomic shells.

In the particular case of lead, bismuth, thorium, and uranium, some previous works were devoted to the study of *M* x-ray emission spectra. Regarding theoretical determinations, Chen and Crasemann [1] calculated relativistic Dirac-Fock transition probabilities for lead and uranium in the frozen orbital approximation. Experimental determinations of uranium $M\alpha$ and $M\beta$ spectra were performed by Keski-Rakkonen and Krause [2] and Ohno *et al.* [3] by means of photoelectron analysis of x rays (PAX) and high-resolution double crystal spectrometry, respectively. In addition, Raboud de Villarsiviriaux and co-workers [4,5] carried out detailed measurements of thorium and uranium *M* spectra by high-resolution x-ray spectroscopy, although they did not provide data for transition probabilities.

In this work, the structure of lead, bismuth, thorium, and uranium *M* x-ray spectra was studied experimentally from x-ray emission induced by electron incidence. Relative transition probabilities, characteristic energies, natural linewidths, and x-ray production cross sections for these elements were determined for a large number of decays toward the *M* shell.

The adequate processing of *M* x-ray spectra requires a cautious fitting procedure in order to achieve an accurate spectral deconvolution. On one hand, the x-ray generation, self-absorption, and detection features must be properly described, and therefore, reliable data of mass absorption coefficients, a good model for bremsstrahlung production, a detailed knowledge of detection artifacts, etc., must be available. On the other hand, the presence of satellite bands with energies around 10 eV higher than the diagram lines, particularly the $M_5N_7(M\alpha_1)$, $M_4N_6(M\beta)$, and $M_3N_5(M\gamma)$ lines, produces an additional distortion that must be taken into account. Those bands arise from a large number of satellite lines resulting from decays in double vacancy configurations originated by Coster-Kronig (CK) transitions within *M* subshells [2]. The measured spectra were processed by using a robust fitting procedure based on a parameter refinement method [6] which accounts for all the mentioned spectral features.

II. EXPERIMENT

Measurements were performed with a scanning electron microscope LEO 1450VP furnished with a wavelength dispersive spectrometer (WDS) INCA WAVE 700 from the Laboratorio de Microscopía Electrónica y Microanálisis (LABMEM) of the Universidad Nacional de San Luis. The arrangement of the WDS is Johansson type for the PET crys-

TABLE I. Experimental conditions for the analyzed spectra.

Element	Beam current (nA)	Acquisition time (min)	Analyzed range (keV)
Pb	186	85	1.66–4.13
Bi	190	95	1.68–5.00
Th	125	68	2.07–5.00
U	186	53	2.36–5.00

tal (d=4.37 Å) used in this work. The x rays diffracted by the analyzing crystal are collected by two proportional counters operated in tandem: the first of them is a P10 (90% Ar-10% CH_4) flow counter and the second one is a sealed Xe counter.

Lead, bismuth, thorium, and uranium M x-ray spectra were collected from pure standards with an incident beam energy E_o of 15 keV, a take-off angle of 29°, and a collimator slit size of 0.1 mm. The other experimental conditions are summarized in Table I.

To take into account the influence of possible beam instability, fluctuations in the beam current were monitored from the variations registered for the specimen current on the basis of the constant relationship between them for a given atomic number and incidence energy. It was necessary to perform this procedure since a direct measurement of the beam current during spectra acquisition is not possible.

III. SPECTRAL ANALYSIS

The atomic parameters sought were obtained from the characteristic M-line positions, shapes, and relative intensities. The spectral processing involves the fitting of a function which describes the spectrum adequately, i.e., each peak shape and the bremsstrahlung, taking into account detection artifacts, spectrometer efficiency, and the absorption of radiation within the specimen. For this purpose, an optimization method of atomic and experimental parameters was implemented for the processing of x-ray spectra emitted by a specimen after electron bombardment and collected with a WDS.

A. Analytical description of spectra

The analytical function proposed to fit the experimental spectra involves a number of parameters to be optimized by means of a minimization procedure. The calculated intensity at the energy E_i corresponding to the spectral channel i can be written as

$$\tilde{I}_i = B(E_i) + \sum_q P_q V_q(E_i), \tag{1}$$

where B accounts for the bremsstrahlung registered by the spectrometer, P_q is the detected characteristic intensity of the line q, and V is a Voigt profile used to describe the characteristic peak shape.

1. Bremsstrahlung

The expression $B(E)$ for the description of the bremsstrahlung as a function of the photon energy E, the average atomic number $\bar{Z}$, and the incident electron energy E_o is given by Ref. [7],

$$B(E) = \sqrt{\bar{Z}}\frac{(E_o - E)}{E}\alpha A R \varepsilon(E)\left(-73.90 - 1.2446E + 36.502 \ln \bar{Z} + \frac{148.5E_o^{0.1293}}{\bar{Z}}\right) \times \left(1 + (-0.006624 + 0.0002906E_o)\frac{\bar{Z}}{E}\right), \tag{2}$$

where the energy is in keV, α is a constant proportional to the number of incident electrons, A is the absorption correction, R accounts for intensity losses due to backscattered electrons, and ε is the spectrometer efficiency.

2. Characteristic line intensities

The detected characteristic intensity P_q of the line q, generated by an electron transition to the D_l shell of a pure element, can be expressed as

$$P_q = \beta \sigma_l^X p_q (ZAF)_q \varepsilon(E_q), \tag{3}$$

where β is a constant proportional to the number of incident electrons, Z, A, and F are the atomic number, absorption, and fluorescence correction factors, respectively, p_q is the relative transition probability for the line q, E_q is the energy of the line q, and $\sigma_l^X = \tilde{Q}_l \omega_l$ is the x-ray production cross section for the D_l shell at energy E_o (that is to say, the product of the final vacancy production cross section $\tilde{Q}_l$ and the fluorescence yield ω_l for the D_l shell). In the case of transitions to M shells, i.e., $D_l = M_l$, the vacancy production cross section can be written as

$$\begin{aligned}
\tilde{Q}_{M_1} &= Q_{M_1}, \\
\tilde{Q}_{M_2} &= Q_{M_2} + f_{1,2}\tilde{Q}_{M_1}, \\
\tilde{Q}_{M_3} &= Q_{M_3} + f_{1,3}\tilde{Q}_{M_1} + f_{2,3}\tilde{Q}_{M_2}, \\
\tilde{Q}_{M_4} &= Q_{M_4} + f_{1,4}\tilde{Q}_{M_1} + f_{2,4}\tilde{Q}_{M_2} + f_{3,4}\tilde{Q}_{M_3}, \\
\tilde{Q}_{M_5} &= Q_{M_5} + f_{1,5}\tilde{Q}_{M_1} + f_{2,5}\tilde{Q}_{M_2} + f_{3,5}\tilde{Q}_{M_3} + f_{4,5}\tilde{Q}_{M_4},
\end{aligned} \tag{4}$$

where Q_{M_l} is the ionization cross section for the M_l subshell and $f_{n,l}$ is the Coster-Kronig transition probability for an initial state with a vacancy in the M_n subshell and a final state with a vacancy in the M_l subshell. In the expressions given above, the generation of vacancies in the M shells due to Auger or radiative transitions occurring towards L or K shells were neglected, since the probability of generating vacancies is null for the K shell and negligible for L shells at E_o=15 keV. Vacancies created in M shells due to super-Coster-Kronig transitions were also not considered, because they are not energetically possible for the elements studied.

Regarding Z, A, and F corrections, a model for the ionization distribution function $\Phi(\rho z)$ previously developed [8]

(based on the description given by Packwood and Brown [9]), was used in the present calculations. Notice that the absorption and fluorescence corrections are close to unity for spectra from pure elements, and therefore they are of less importance in Eq. (3).

3. Peak shape

A Voigt profile was used to describe the characteristic peak shape (which is strongly dependent on the detection system). This Voigt function is the convolution of two probability distributions: a Gaussian G associated to the spectrometer response and a Lorentzian L, whose width is related to the lifetime of the initial hole state [10],

$$V(x) = \int_{-\infty}^{\infty} G(x')L(x-x')dx', \tag{5}$$

where

$$G(x') = \frac{\sqrt{\ln 2}}{\sqrt{\pi}\gamma_G} \exp[-\ln 2(x'/\gamma_G)^2] \tag{6}$$

and

$$L(x-x') = \frac{1}{\pi\gamma_L} \frac{\gamma_L^2}{[(x-x')^2+\gamma_L^2]}, \tag{7}$$

with γ_G and γ_L the half widths at half maximum of the Gaussian and Lorentzian, respectively.

A simple expression for the Voigt function, developed in terms of the complementary error function with complex arguments, and expressed in terms of series of trigonometric and hyperbolic functions with real arguments, was used, along with a very simple asymptotic expansion [11].

The instrumental resolution γ_G is governed by the angular divergence $\Delta\theta$ of the analyzer crystal and it can be derived from the Bragg's law,

$$\gamma_G = \Delta\theta E \sqrt{\left[\left(\frac{2d}{hc}E\right)^2 - 1\right] 2\ln 2}, \tag{8}$$

where d is the interplanar spacing of the crystal, h is the Planck's constant, and c is the speed of light in vacuum. The value of γ_G in Eq. (8) is a lower limit for the instrumental resolution, since defocusing problems and, at a lower extent, the width of the rocking curve of the crystal, contributes to the experimental peak broadening [12].

B. Spectrometer efficiency

The spectrometer efficiency ε, appearing in Eqs. (2) and (3), was determined according to a method recently developed which only requires experimental data [13]. This method is based on the comparison of two measurements of the same bremsstrahlung spectrum: one of them performed with an energy dispersive spectrometer (EDS), and the other one, with the wavelength dispersive spectrometer (WDS) whose efficiency is to be determined. A good approach to the WDS efficiency is given by the ratio of these two measurements multiplied by the EDS efficiency, which may be estimated with a reasonable degree of accuracy. The dependence of ε with E is well described by the following second-order polynomial [13]:

$$\varepsilon = 0.00014 - 0.00018E + 0.000174E^2, \tag{9}$$

where the photon energy is expressed in keV.

C. Optimization procedure

The optimization method implemented for WDS spectral processing was previously developed for EDS [6]. This method consists in minimizing the quadratic differences between the experimental spectrum to be fitted and the analytical function proposed to describe it [Eq. (1)], by optimizing the parameters involved in the analytical prediction. The quantity to be minimized can be written as

$$\chi^2 = \frac{1}{N_c - N_p} \sum_{i=1}^{N_c} \frac{(\tilde{I}_i - I_i)^2}{I_i}, \tag{10}$$

where I_i and $\tilde{I}_i$ are, respectively, the experimental and calculated intensities for the energy E_i corresponding to channel i, N_c is the total number of channels, and N_p is the number of parameters to be refined. Thus, atomic and experimental quantities are obtained as a result of the optimization procedure, after the refinement of the corresponding parameters, carried out through a cautious sequence of minimization steps in order to obtain the best possible fit of the experimental spectrum.

In order to assess the uncertainties related to the parameters refined, the intensity registered for each spectral channel is considered as a stochastic variable obeying Poisson statistics; i.e., its standard deviation is given by the square root of its mean value. The errors associated to the optimized parameters are then obtained by propagating the errors in the channel intensities by numerical differentiation [14].

IV. RESULTS AND DISCUSSION

A general good fit of all the experimental spectra was achieved. As an example, Fig. 1 shows the measured uranium spectrum along with the corresponding analytical description.

In the following sections, the relative transition probabilities, characteristic energies, natural linewidths, and x-ray production cross sections obtained from the spectral fitting procedure are presented. Finally, a characterization of the satellite bands due to spectator hole transitions is given.

A. Relative transition probabilities

The transition probability associated to a line M_lX_j, relative to all the transitions to the M_l subshell, referred to as the M_lX_j relative transition probability, was determined from the measured spectra for several lines and the four elements studied. The values obtained for these relative transition probabilities are shown in Table II. The theoretical predictions given by Chen and Crasemann [1] for U and Pb and the ones published by Perkins *et al.* [15] for Th and Bi are also

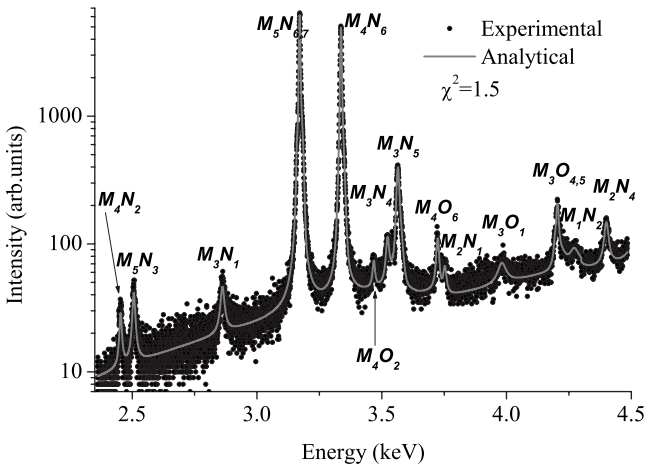

FIG. 1. Experimental and analytical x-ray spectra of uranium.

presented for comparison. Although the latter were obtained by interpolating theoretical data, they were included in Table II due to the lack of data in the literature for these transitions.

In most of the transitions investigated (34 of 52), differences lower than 20% respect to the data reported by the other authors were found, whereas the discrepancies are between 20% and 50% for 11 values and greater than 50% for the remainder 7 cases.

Regarding the most probable decays, a general agreement was observed (differences are smaller than 8% for the M_5, M_4, and M_3 subshells and smaller than 12% for the M_2 and M_1 subshells), with the exception of the decays to uranium M_2 subshell, where great deviations can be seen. A similar disagreement can also be found among theoretical treatments: according to data published by Bhalla [16], the relative M_2N_1 transition probability of Yb, Hg, and Np lies between 0.23 and 0.27; nevertheless, although a value within this interval would be expected for uranium, Chen and Crasemann [1] gave a value of 0.14 for this element. It must be taken into account that a possible satellite band at the high energy side of the M_4O_6 peak would explain the important departures from the theoretical predictions.

In addition to the M_2N_1 line, theoretical results from different authors for other main transitions present important discrepancies. In Fig. 2, the experimental results obtained in the present work are compared with the data published by Chen and Crasemann and by Bhalla for the most intense lines associated to each subshell. Chen and Crasemann [1] carry out relativistic Dirac-Fock calculations in the approximation of frozen orbital performed in the length gauge to obtain M x-ray emission rates. Bhalla [16] uses the relativistic Hartree-Fock-Slater frozen-core atomic model including finite nuclear size and retardation effects. As can be seen from Fig. 2, the disagreement between both theoretical models is very significant. The differences between the data obtained here and the results published by Chen and Crasemann are less than the discrepancies between both calculations. Therefore, the present experimental data corroborate the model used by those authors.

The transitions indicated with dotted lines in Table II belong to lines observed in the spectra with very low statistics or overlapped with other peak; for this reason, data published in the literature (Ref. [1] for Pb and Ref. [15] for Bi) were considered for normalization in the corresponding subshell.

TABLE II. Relative transition probabilities for Pb, Bi, Th, and U M decays. Numbers in parentheses indicate the estimated uncertainties in the last digit. Results obtained in the present work are compared with theoretical data given by Chen and Crasemann [1] and Perkins *et al.* [15].

	Pb		Bi		Th		U	
Transition	This work	Ref. [1]	This work	Ref. [15]	This work	Ref. [15]	This work	Ref. [1]
M_5N_3	0.026(2)	0.037	0.023(1)	0.041	0.027(1)	0.031	0.034 (1)	0.030
M_5N_6	0.05 (1)	0.047	0.042(8)	0.047	0.040(3)	0.047	0.035 (2)	0.047
M_5N_7	0.93 (2)	0.917	0.94 (1)	0.912	0.933(7)	0.922	0.931 (5)	0.923
M_4N_2	0.013(3)	0.045	0.016(2)	0.054	0.023(2)	0.043	0.032 (2)	0.042
M_4N_6	0.987(8)	0.955	0.971(7)	0.933	0.965(7)	0.947	0.940 (3)	0.935
M_4O_2			⋯	0.013	0.012(1)	0.010	0.0086(9)	0.009
M_4O_6							0.019 (1)	0.014
M_3N_1	⋯	0.163	0.117(8)	0.165	0.18 (1)	0.170	0.172 (8)	0.166
M_3N_4	0.07 (1)	0.081	0.08 (1)	0.080	0.052(6)	0.081	0.104 (4)	0.078
M_3N_5	0.63 (2)	0.624	0.62 (3)	0.618	0.66 (2)	0.607	0.54 (2)	0.583
M_3O_1	0.03 (1)	0.032	0.077(9)	0.036			0.087 (6)	0.039
$M_3O_{4,5}$	⋯	0.101	0.106(6)	0.101	0.111(3)	0.143	0.096 (8)	0.135
M_2N_1							0.36 (3)	0.140
M_2N_4			0.70 (5)	0.721	0.73 (4)	0.678	0.46 (2)	0.674
M_2O_4			0.13 (3)	0.113	0.10 (2)	0.154		
M_1N_2	0.61 (7)	0.552	0.64 (6)	0.573	0.67 (5)	0.633		
M_1N_3	0.39 (5)	0.448	0.36 (6)	0.427	0.33 (4)	0.367		

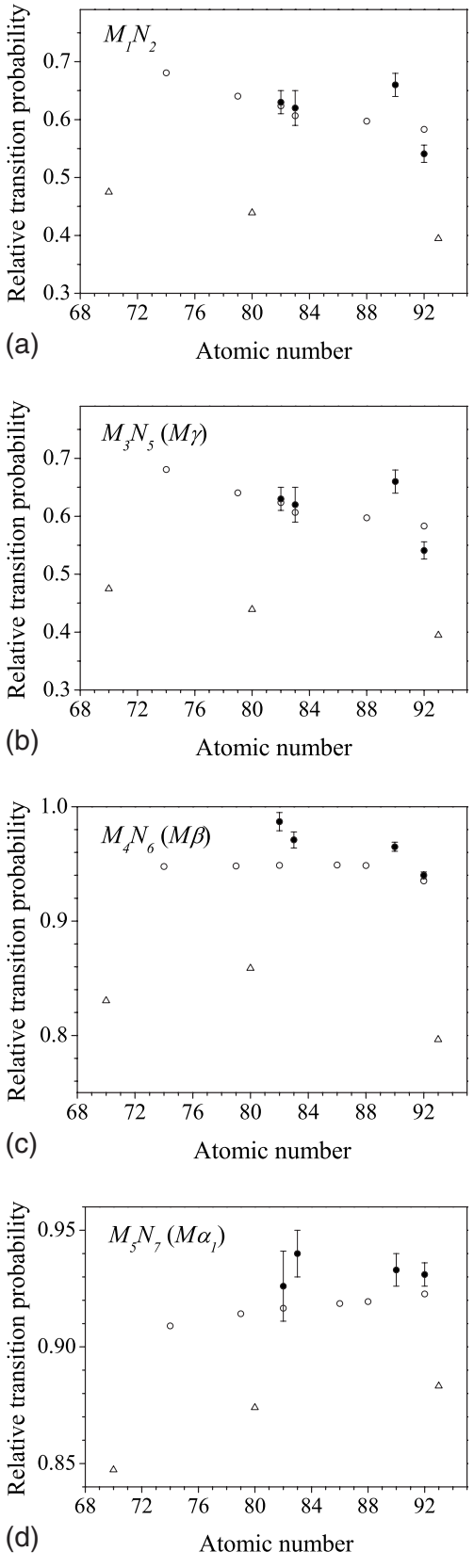

FIG. 2. Relative transition probabilities as a function of the atomic number in the interval [70, 93] for the decays: (a) M_1N_2, (b) M_3N_5, (c) M_4N_6, and (d) M_5N_7 obtained in this work (black circles), given by Chen and Crasemann [1] (hollow circles) and by Bhalla [16] (triangles).

TABLE III. Characteristic energies (in keV) for Pb and Bi *M* transitions. Numbers in parentheses indicate the estimated uncertainties in the last digit. Results obtained are compared with experimental data given by Bearden [17].

	Pb		Bi	
Transition	This work	Ref. [17]	This work	Ref. [17]
M_5N_3	1.8390 (6)	1.8395(8)	1.9009 (3)	1.901 (1)
M_5N_6	2.3417 (6)	2.3397(9)	2.4185 (6)	2.4170(9)
M_4N_2	1.8222 (9)	1.823 (1)	1.8821 (5)	1.883 (1)
M_4N_6	2.44252(2)	2.4427(5)	2.52547(2)	2.5255(5)
M_4O_2			2.5703 (8)	2.571 (2)
M_3N_1			2.2389 (6)	2.239 (3)
M_3N_4	2.625 (2)	2.630 (2)	2.7149 (7)	2.712 (3)
M_3N_5	2.6534 (3)	2.6527(5)	2.7378 (3)	2.735 (1)
M_3O_1	2.919 (5)	2.921 (6)	3.020 (1)	3.021 (7)
$M_3O_{4,5}$	3.0463 (4)	3.047 (4)	3.1558 (4)	3.153 (5)
M_2N_4	3.1181 (6)	3.124 (4)	3.2353 (5)	3.234 (3)
M_2O_4			3.672 (2)	
M_1N_2	3.077 (2)		3.193 (2)	3.185 (7)
M_1N_3	3.207 (2)	3.202 (7)	3.324 (3)	3.315 (8)

The transitions corresponding to decays to the M_2 subshell does not add up to unity, since more lines than the observed ones were taken into account for the normalization. The lines considered were the most intense (M_2N_4) and other three decays with significant probabilities (M_2N_1, M_2O_4, and M_2O_1) according to Chen and Crasemann [1] and Bhalla [16].

For the most intense lines (M_5N_7, M_4N_6, M_3N_5, and $M_3O_{4,5}$) the relative transition probabilities were determined with low uncertainties (less than 8%). Greater uncertainties (up to 30%) are presented for very weak transitions or weak transitions with characteristic energies close to other diagram line or in the vicinity of a spectator hole transition. The first case applies to M_3O_1 and M_1N_3 decays while the second one corresponds to M_5N_6, M_3N_4, and M_1N_2 transitions.

B. Characteristic energies

Characteristic energies for 52 transitions were determined relative to the energy corresponding to the M_5N_7 decay according to Bearden [17]. In Tables III and IV, the values obtained are compared to the experimental data published by that author. As can be seen, both datasets are experimentally undistinguishable within the combined uncertainties except for nine particular transitions: M_5N_6, M_3N_4, $M_3O_{4,5}$, and M_2N_4 for lead, M_3N_5 for bismuth, M_4N_2 and M_3N_1 for thorium, and M_3N_4 and M_2N_1 for uranium, where differences are lower than 0.2% for the eight first transitions and equal to 0.7% for U M_2N_1. Regarding this last particular case, a better agreement with the data published by Bearden would be found if the close uranium lines M_2N_1 and M_4O_6 were interchanged. Nevertheless, if this choice were made, an unrealistically narrow peak would result for the first one, with a natural linewidth of 9 eV, i.e., considerably smaller than any

TABLE IV. Characteristic energies (in keV) for Th and U M transitions. Numbers in parentheses indicate the estimated uncertainties in the last digit. Results obtained are compared with experimental data given by Bearden [17].

	Th		U	
Transition	This work	Ref. [17]	This work	Ref. [17]
M_5N_3	2.3641 (3)	2.364 (2)	2.5062 (3)	2.507 (1)
M_5N_6	2.9869 (3)	2.987 (1)	3.1603 (3)	3.1595(8)
M_4N_2	2.3220 (5)	2.322 (2)	2.4534 (4)	2.455 (1)
M_4N_6	3.14580(3)	3.1458(8)	3.33634(3)	3.3367(9)
M_4O_2	3.2572 (8)	3.256 (3)	3.4685 (8)	3.467 (1)
M_4O_6			3.7239 (3)	
M_3N_1	2.7176 (6)	2.714 (3)	2.8614 (5)	2.863 (1)
M_3N_4	3.342 (1)	3.335 (3)	3.5232 (4)	3.521 (2)
M_3N_5	3.3703 (2)	3.370 (2)	3.5639 (2)	3.563 (1)
M_3O_1			3.980 (3)	3.980 (9)
$M_3O_{4,5}$	3.9590 (3)	3.959 (4)	4.2035 (3)	4.205 (3)
M_2N_1			3.751 (1)	3.724 (4)
M_2N_4	4.1168 (6)	4.117 (3)	4.4000 (5)	4.401 (3)
M_2O_4	4.739 (1)	4.735 (9)		
M_1N_2	4.012 (1)		4.272 (2)	4.25 (3)
M_1N_3	4.221 (2)	4.23 (1)		

of the involved level widths [18]. It must be emphasized that the uranium M_4O_6 transition is not included in Ref. [17] and that this line is less energetic than M_2N_1 according to Ref. [15], which agrees with the data obtained here.

In all the cases the uncertainties estimated here were lower or equal to the corresponding ones published by Bearden. In addition, four characteristic energy values (corresponding to Pb M_1N_2, Bi M_2O_4, Th M_1N_2, and U M_4O_6 transitions) not published in Ref. [17] were determined in the present work.

C. Natural linewidths

In order to obtain the natural linewidths $2\gamma_L$ introduced in Eq. (7), the instrumental resolution γ_G was previously determined. This parameter is related with the angular divergence $\Delta\theta$ as indicated in Eq. (8) and it is almost constant for the Johansson arrangement [12]. To determine the "constant" $\Delta\theta$, the values of γ_G obtained with the optimization algorithm for lead, bismuth, thorium, and uranium M_4N_6 lines, were fitted using the function given by Eq. (8). These lines were chosen, although a satellite structure exists, because of their good statistics; another possible option could have been the M_5N_7 transitions, but they were disregarded because, in addition to the presence of a spectator hole multiplet, they are strongly overlapped with the M_5N_6 lines. Finally, with the value obtained for $\Delta\theta$, the parameter γ_L was determined from the fitting process for 40 of the transitions studied. The corresponding natural linewidths are shown in Tables V and VI compared with other experimental and theoretical values.

Different complications arise in the determination of the natural linewidths; the most important are indicated in the tables. For example, the main transition M_5N_7 is affected by the influence of the line M_5N_6 and by the proximity of a satellite band at the high-energy side originated by spectator hole transitions. Similar bands affect also the lines M_4N_6,

TABLE V. Natural linewidths (in eV) corresponding to Pb, Bi, and Th M transitions. The results obtained are compared with other experimental and theoretical determinations. Numbers in parentheses indicate the estimated uncertainties in the last digit.

	Pb		Bi		Th			
Transition	This work	Ref. [18]	This work	Refs. [18,19]	This work	Ref. [5]	Refs. [20,21]	Refs. [18,19]
M_5N_3	13 (2)	8.1	8.1 (8)	8.4	9.4 (8)	14.3(7)	10.4	10.6
M_5N_7	2.88(5)[a]	2.8	3.07(4)[a]	2.9	4.16(5)[a]	3.5(1)	3.1	3.5
M_4N_2	8 (2)	9.6	7 (1)	10.2	9 (1)	17 (1)	11.5	10.6
M_4N_6	3.04 (4)	2.8	3.11 (3)	2.9	4.15 (2)	3.5(1)	3.4	3.5
M_4O_2			12 (2)	4.6[b]	12 (2)			8.1[b]
M_3N_1			15 (2)	17.7	19 (2)			18.8
M_3N_4			8 (2)	12.1				
M_3N_5	12.7 (7)	11.9	12.3 (6)	11.9	13.1 (4)[c]	12.1(6)	18.2	11.5
M_3O_1			22 (3)					
$M_3O_{4,5}$	7.0 (9)		9 (1)	8.2[b]	10.4 (8)	7.7(1)		8.3[b]
M_2N_4			17 (2)	15.8	22 (2)	17.7(2)	20.8	18.6
M_2O_4			17 (4)	12.1[b]	10 (4)			15.1[b]
M_1N_3			29 (7)	23.7				

[a]Doublet and spectator hole band.
[b]Linewidths estimated by using the O-shells widths given by Fuggle and Alvarado [19].
[c]Two satellite structures.

TABLE VI. Natural linewidths (in eV) corresponding to U *M* transitions. The results obtained are compared with other experimental and theoretical determinations. Numbers in parentheses indicate the estimated uncertainties in the last digit.

	U					
Transition	This work	Ref. [5]	Ref. [2]	Ref. [3]	Refs. [20,21]	Refs. [18,19]
M_5N_3	13.2 (8)	12.8(3)	15 (2)		10.8	11.1
M_5N_7	4.87(4)[a]	3.5(1)	4.1(3)	3.8(2)	4.45	3.8
M_4N_2	11 (1)	15 (1)	13 (2)		11.9	12.6
M_4N_6	4.83 (4)	3.6(1)	4.3(3)	3.9(2)	4.7	3.8
M_4O_2	11 (2)					8.0[b]
M_4O_6	8.2 (8)					
M_3N_1	20 (1)	20.2(8)			24.4	19.1
M_3N_5	11.3 (3)[c]		14[d]			11.5
$M_3O_{4,5}$	9 (1)	8.2(1)				8.4[b]
M_2N_1	19 (2)					27.3
M_2N_4	18 (1)	18.1(2)			24.4	19.8

[a]Doublet and spectator hole band.
[b]Linewidths estimated by using the *O*-shells widths given by Fuggle and Alvarado [19].
[c]Two satellite structures.
[d]Line distorted by M_5 absorption edge.

M_3N_5, and $M_3O_{4,5}$, as explained in Sec. IV E. Another problem arises in relation to the transition M_3N_5: between this decay and the M_3N_4 one there is a broad structure that, for uranium and thorium, may be attributed to a M_5P_1 quadrupole transition, and several unresolved lines tentatively assigned to the M_3N_4N satellite and to the M_4O_3 and M_5P_3 transitions [5]. A reliable determination of the M_3N_4 natural linewidths could not be performed for lead, thorium and uranium because of these problems; therefore they were not included in Tables V and VI.

The uranium linewidths obtained were compared with results obtained by high-resolution x-ray spectroscopy [5], with experimental values measured by PAX [2]; and with linewidths measured by high-resolution double crystal x-ray spectroscopy [3]. The theoretical linewidths given in the sixth column of Table VI were obtained by Raboud *et al.* [5] by adding the widths of the *M* and *N* levels involved in each transition, taken from McGuire's predictions (Refs. [20,21], respectively).

The value for γ_L given by Keski-Rakhonen and Krause [2] for the M_3N_5 ($M\gamma$) line is indicated by these authors as distorted by the M_5 absorption edge. This inconvenience was overcome in this work by taking into account all the absorption edges involved in the analytical description of the spectra.

Thorium *M* linewidths were also compared with the results measured and calculated in Ref. [5]. No data were found in the literature for lead and bismuth; for this reason, an estimation was carried out by adding the level widths involved according to the fit of experimental results compiled by Campbell and Papp [18] with Fuggle and Alvarado [19] *O*-shell widths. This procedure was also used as an additional source of data for uranium and thorium.

As can be observed from Tables V and VI, there is a great discrepancy among the different linewidth determinations available in the literature, even for the most intense lines. Although the values presented here agree with the other data in the 70% of the cases considering the combined uncertainties (assumed to be 0.1 eV in the values obtained by adding level widths), there is a great discrepancy for some intense lines. For this reason, a more detailed study should be carried out to achieve more precise data.

Raboud *et al.* [5] performed the fitting of uranium and thorium spectra in narrow energy regions. They include one or two Voigt profiles for the spectator hole multiplets, without giving a clear justification of the criterion used for each case. Other authors [2,3], instead of fitting the satellite structure along with the parent lines, only fit the main lines and assign the residuals to this satellite band. This strategy introduces a systematic overestimation in the diagram line intensity, since the low energy tail of the satellite structure is accounted for as a part of the main peak. The present fitting method is based on a minimization process carried out in a wide spectral range considering jointly both diagram lines and satellite structures (see Sec. IV E).

The good energy resolution of the spectrometers used in some of the previous works is not sufficient to obtain precise values for γ_L, since these natural linewidths are large enough to complicate the deconvolution in certain cases, particularly for peaks accompanied by satellite structures. A robust fitting method is also necessary in order to take into account most of the involved processes in a realistic way. In this sense, the parameter refinement method used in this application, which involves Voigt profiles for the description of peak shapes, has shown a very good performance.

D. X-ray production cross section

The x-ray production cross section $\sigma^X_{M_l}$ for the M_l subshell is the product of the final vacancy production cross section

TABLE VII. X-ray production cross sections relative to the M_5 subshell for 15 keV electrons. Numbers in parentheses indicate the estimated uncertainties in the last digit

	Pb	Bi	Th	U
$\sigma^X_{M_1}/\sigma^X_{M_5}$	0.073(6)	0.054(4)	0.036(2)	
$\sigma^X_{M_2}/\sigma^X_{M_5}$	0.057(8)	0.06 (2)	0.04 (1)	0.058(8)
$\sigma^X_{M_3}/\sigma^X_{M_5}$	0.26 (3)	0.25 (4)	0.21 (2)	0.23 (2)
$\sigma^X_{M_4}/\sigma^X_{M_5}$	0.82 (5)	0.78 (4)	0.69 (4)	0.68 (3)

$\tilde{Q}_{M_l}$ and the fluorescence yield ω_{M_l}, as mentioned in Sec. III A 2. This parameter varies with the incident particle energy through the magnitude $\tilde{Q}_{M_l}$; in addition, it depends on the kind of exciting particle. In the present work, an estimation for $\sigma^X_{M_l}$ relative to $\sigma^X_{M_5}$ for 15 keV electrons is carried out for the M subshells studied. In this approach, a constant electron energy E_o is assumed, although the electron energy E capable to ionize varies from E_o to the atomic level energy E_{M_l} in the thick standards used. In view of the lack of data published for $\sigma^X_{M_l}$, this approximation can serve as a basis for further theoretical or experimental determinations. The results obtained are displayed in Table VII. A monotonic increase towards less bound atomic levels is observed for all the elements studied (except for M_1 lead cross section). This behavior was expected since, as can be seen from Eq. (4), the more external the atomic shell, the greater the final vacancy production cross section $\tilde{Q}_{M_l}$. This increase in $\tilde{Q}_{M_l}$ is due to two reasons: on the one hand, the ionization cross section Q_{M_l} is greater for more external shells because they have a larger number of electrons which, in addition, are less tightly bound. On the other hand, for less tightly bound levels, there are more combinations of Coster-Kronig processes able to generate secondary vacancies. Taking into account the slight variation found for ω_{M_l} for different subshells (around 15%, according to Ref. [15]) as compared to the variations for the x-ray production cross sections shown in Table VII, it is reasonable to conclude that its behavior is mainly given by $\tilde{Q}_{M_l}$.

E. Spectator hole transitions

In Fig. 3, lead, bismuth, and uranium spectra in the regions involving the $M\alpha$, $M\beta$, and $M\gamma$ transitions, respectively, are shown. The fitting curves, the contributions of each diagram line and the associated satellite bands, are also displayed. These spectator hole multiplets at the high-energy side of the diagram lines were fitted with Gaussian profiles with different amplitudes, widths, and positions. As can be seen in Fig. 3, these structures are well described by only one Gaussian function. The more complicated structure between M_3N_4 and M_3N_5 lines, mentioned in Sec. IV C, can be observed in Fig. 3(c). The energy shift ΔE respect to the main transition, the full width at the half maximum (FWHM), and the intensity relative to the whole peak (satellite and parent line) are shown in Table VIII for all the multiplets studied.

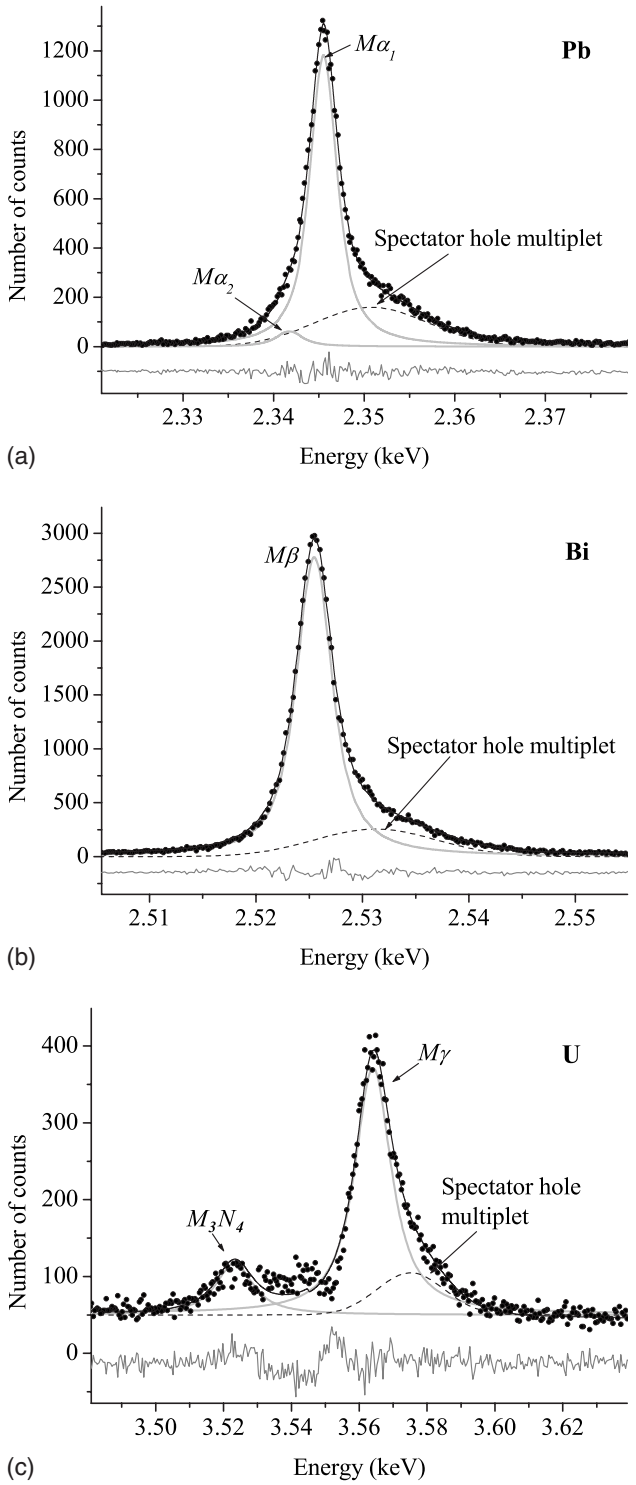

FIG. 3. Lead (a), bismuth (b), and uranium (c) spectra in the regions corresponding to $M\alpha$, $M\beta$, and $M\gamma$, respectively. Dots, experimental, black solid line, fitting curves; light gray thick solid lines, diagram lines; dashed lines, spectator hole band; and gray thin solid lines, residuals.

The main mechanism in the generation of these bands is the emission of an electron from the N shell after a CK transition within the M shell. When the doubly ionized atom decays to fill the M vacancy, the energy levels are altered due

TABLE VIII. Characteristic parameters of the satellite structures associated to $M\alpha_1$, $M\beta$, and $M\gamma$ transitions for lead, bismuth, thorium, and uranium, for 15 keV electron excitation. Numbers in parentheses indicate the estimated uncertainties in the last digit.

	Satellite structure			
	Diagram line	ΔE (eV)	FWHM (eV)	Relative area (%)
Pb	M_5N_7	5.2(1)	14.7 (2)	28.9 (8)
	M_4N_6	6.0(1)	13.1 (2)	19 (1)
Bi	M_5N_7	5.5(1)	15.8 (2)	27.0 (7)
	M_4N_6	5.7(1)	13.5 (2)	19 (4)
	M_3N_5	10.8(1)	28 (3)	16 (4)
Th	M_5N_7	6.7(1)	17.8 (2)	20.1 (5)
	M_4N_6	6.0(1)	16.8 (1)	16 (2)
	M_3N_5	13.0(1)	13 (2)	5 (2)
	$M_3O_{4,5}$	13.0(1)	60 (10)	40 (10)
U	M_5N_7	10.1(1)	13.3 (2)	10.4 (3)
	M_4N_6	6.5(1)	18.7 (4)	13 (2)
	M_3N_5	11.0(1)	24 (1)	18 (3)
	$M_3O_{4,5}$	11.0(1)	47.1 (6)	37 (7)

to the N spectator hole and then, the characteristic photon is emitted with an energy slightly greater than that corresponding to the diagram line. The energy shift depends on the shell to which the spectator hole belongs: for uranium, this structure is centered at an energy around 6–10 eV higher than the main line for both $M\alpha_1$ and $M\beta$ lines, according to theoretical calculations performed by Keski-Rahkonen and Krause. When the incident beam energy is sufficient to ionize the L shell, an Auger LMM decay could occur leaving the atom in a double M vacancy state with a stronger distortion of levels, producing an energy shift greater than 50 eV. This case, however, is not possible for uranium and thorium and is very improbable for bismuth and lead in the present experiment, since the excitation energy is only 15 keV. Another mechanism of decay is the shakeoff, for which a second electron is ejected from a more external shell (O, P, or Q, for the heaviest elements) without CK transitions. This second vacancy distorts very weakly the atomic energy levels; thus, the characteristic photon completing the decay is emitted with an energy almost equal to that of the main line ($\Delta E < 1$ eV) from which it is usually undistinguishable [3].

As can be seen in Table VIII, the energy shift ΔE respect to the main transition increases with the atomic number for the M_5N_7 satellite band, from 5.2 eV for lead to 10.1 eV for uranium; while for the structures associated to the other diagram lines, this shift does not show any tendency. The results obtained for uranium are in good agreement with the data published by Keski-Rahkonen and Krause for the satellite band related to M_5N_7 and M_4N_6 lines.

Regarding the band widths, it can be observed that multiplets involving M_3 subshell are appreciably broader than the other ones, with the exception of the satellite related to Th M_3N_5. In order to obtain more conclusive results about this issue, it would be necessary to have reliable theoretical data about multiplet energy distributions for an adequate location of their centroids

The relative area decreases with the atomic number for satellite spectator hole multiplets associated to the M_5N_7 and M_4N_6 diagram lines. Due to the lack of data available in the literature, only uranium M_5N_7 and M_4N_6 multiplets can be compared. The present values of relative areas (10.4% and 13% for M_5N_7 and M_4N_6 satellite bands, respectively) are in good agreement with the results obtained by Keski-Rahkonen and Krause with 12 keV electron excitation, (11 ± 2)% for both bands. On the other hand, Ohno *et al.* [3] found relative areas of 33% and 11% for these spectator hole transitions with photon excitation by using a Mo x-ray tube. This excitation source (unlike the 15 keV electron beam) enables L-shell ionization and consequently, allows the generation of M spectator holes by LMM Coster-Kronig and LMN Auger transitions, which strongly affects the band structure.

V. CONCLUSION

Different parameters involving decays to the M shell were experimentally determined for lead, bismuth, thorium, and uranium from 15 keV electron induced x-ray spectra. The parameters investigated include relative transition probabilities, characteristic energies, natural linewidths, x-ray production cross sections, and characteristic parameters of spectator hole multiplets.

Relative probabilities of 52 atomic transitions were determined for which no previous experimental data are available, except for the most intense uranium characteristic lines [2]. Some of the data obtained are in good agreement with theoretical results from other authors, while important discrepancies were found for some of the less probable transitions. Similar or even greater differences can also be found between the results obtained with different theoretical models [1,16]. The values presented here shows a better agreement with the theoretical prediction given by Chen and Crasemann.

Regarding characteristic energies, values for 52 decays were obtained, showing an excellent agreement with experimental data published by Bearden [17], and lower uncertainties. In addition, four characteristic energy values (Pb M_1N_2, Bi M_2O_4, Th M_1N_2, and U M_4O_6) not published by this author were determined.

The results for natural linewidths obtained here are in reasonable agreement with the data given by other authors, which present a great dispersion among themselves. In addition, linewidths for three transitions not previously published according to our knowledge were obtained as follows: U M_4O_6, Bi M_3O_1, and Pb $M_3O_{4,5}$. Although the first two linewidths were obtained from very weak transitions (therefore, with low statistics), they serve as initial estimations for further determinations.

The x-ray production cross section values obtained show the expected increase for more external levels. Although these parameters were determined for thick samples, and therefore they cannot be directly compared with theoretical data, they are very useful for the analytical description of

spectra from semi-infinite samples, because they take into account all the physical process of vacancy creation.

A simple Gaussian profile was sufficient to properly model the spectator hole band associated to the main characteristic transitions, bearing in mind that a full realistic theoretical description is not available. The results obtained show a good agreement with the behavior observed by Keski-Rakkonen and Krause [2] for the satellites related to M_5N_7 and M_4N_6 uranium decays. This work contributes with the characterization of M_3N_5 and $M_3O_{4,5}$ multiplets for uranium and, in addition, with the description of similar structures associated to thorium, bismuth, and lead main transitions. The corresponding Gaussian parameters (amplitude, width, and position), given for the present particular experimental conditions, serve as a tool for spectral modeling and to test different theoretical approaches.

ACKNOWLEDGMENTS

Financial support by the Consejo Nacional de Investigaciones Científicas y Técnicas and the Agencia Nacional de Promoción Científica y Tecnológica of the Argentine Republic is gratefully acknowledged.

[1] M. H. Chen and B. Crasemann, Phys. Rev. A **30**, 170 (1984).
[2] O. Keski-Rahkonen and M. Krause, Phys. Rev. A **15**, 959 (1977).
[3] M. Ohno, A. Laakkonen, A. Vuoristo, and G. Graeffe, Phys. Scr. **34**, 146 (1986).
[4] P. A. Raboud de Villarsiviriaux, Ph.D. thesis, Université de Fribourg, 2001.
[5] P. A. Raboud, J. C. Dousse, J. Hoszowska, and I. Savoy, Phys. Rev. A **61**, 012507 (1999).
[6] R. Bonetto, G. Castellano, and J. Trincavelli, X-Ray Spectrom. **30**, 313 (2001).
[7] J. Trincavelli and G. Castellano, Spectrochim. Acta, Part B **63**, 1 (2008).
[8] J. A. Riveros, G. Castellano, and J. Trincavelli, Mikrochim. Acta, Suppl. **12**, 99 (1992).
[9] R. Packwood and J. Brown, X-Ray Spectrom. **10**, 138 (1981).
[10] G. Rémond, R. Myklebust, M. Fialin, C. Nockolds, M. Phillips, and C. R. Carmes, J. Res. Natl. Inst. Stand. Technol. **107**, 509 (2002).
[11] S. Limandri, R. Bonetto, H. O. Di Rocco, and J. Trincavelli (unpublished).
[12] S. J. B. Reed, *Electron Microprobe Analysis* (Cambridge University Press, Cambridge, 1993), pp. 71–74.
[13] J. Trincavelli, S. Limandri, A. Carreras, and R. Bonetto, Microsc. Microanal. **14**, 306 (2008).
[14] R. Bonetto, A. Carreras, J. Trincavelli, and G. Castellano, J. Phys. B **37**, 1477 (2004).
[15] S. Perkins, D. Cullen, M. Chen, J. Hubbell, J. Rathkopf, and J. Scofield, Lawrence Livermore National Laboratory Report No. UCRL-50400, 1991 (unpublished), Vol. 30.
[16] C. Bhalla, J. Phys. B **3**, 916 (1970).
[17] J. Bearden, Rev. Mod. Phys. **39**, 78 (1967).
[18] J. Campbell and T. Papp, X-Ray Spectrom. **24**, 307 (1995).
[19] J. C. Fuggle and S. F. Alvarado, Phys. Rev. A **22**, 1615 (1980).
[20] E. McGuire, in *Proceedings of the International Conference on Inner Shell Ionization Phenomena and Future Applications, Atlanta, 1972*, edited by R. Flink, S. Manson, J. Palms, and P. Rao (National Technology Information Service, U.S. Department of Commerce, Springfield, VA, 1973), p. 662.
[21] E. McGuire, Phys. Rev. A **9**, 1840 (1974).